Supplementary Material

Materials and Methods

Oligonucleotides

Guide RNAs:
Sod1: 5' p-rUrUrCrArCrArUrUrGrCrCrCrArArGrUrCrUrCrUrU 3';
miR-122: 5' p-rUrGrGrArGrUrGrUrGrArCrArArUrGrGrUrGrUrUrG 3'

2'OMethyl Capture oligos:
Sod1: 5' Biotin-
mUmCmUmUmCmCmCmAmCmGmAmCmUmUmCmAmUmAmAmAmUmGm
UmGmAmAmAmCmCmUmU 3'
miR-122: 5' Biotin-
mUmCmUmCmUmGmCmUmAmAmCmCmAmUmGmCmGmAmAmCmA
mCmUmCmCmAmUmCmUmCmUmGmC 3'

Competitor DNAs:
Sod1: 5' AAGGTTTCACATTTATGAAGTCGTGGGAAGA 3'
miR-122*:* 5' GCAGAGATCAAGTGTTCGCATGGTTAGCAGAGA 3'

Crystallized Target RNAs:
5' rCrArArUrGrUrGrArArArArA 3';
5' rArArArUrGrUrGrArArArArA 3';
5' rArCrArUrGrUrGrArArArArA 3';
5' rCrCrArArArUrGrUrGrArArArArA 3';

Slicing Targets and Northern Blot Probes:
Sod1: 5'
rArArUrUrArArArArArArGrArGrArCrUrUrGrGrGrCrArArUrGrUrGrArCrArCrCrUrUrAr
A 3'
miR-122: 5' CAAACACCATTGTCACACTCCA 3'

Binding Assay Target RNAs:
Sod1:
5' rUrCrCrCrUrUrArCrGrArCrGrCrArArUrGrUrGrArArArA 3';
5' rUrCrCrCrUrUrArCrGrArCrCrCrArArUrGrUrGrArArArA 3';
5' rUrCrCrCrUrUrArCrGrArCrCrCrArArArUrGrUrGrArArArA 3';
5' rUrCrCrCrUrUrArCrGrArCrCrCrArCrArUrGrUrGrArArArA 3';

miR-122:
5' rArCrCrUrGrCrArGrUrCrGrUrUrCrArCrArCrUrCrCrArArA 3';
5' rArCrCrUrGrCrArGrUrCrGrUrCrCrArCrArCrUrCrCrArArA 3';
5' rArCrCrUrGrCrArGrUrCrGrUrCrArArCrArCrUrCrCrArArA 3';
5' rArCrCrUrGrCrArGrUrCrGrUrCrArUrCrArCrUrCrCrArArA 3';

Protein Expression and Purification

Full length human Ago2 was cloned into pFastBac HT A for expression using the bac-2-bac (Invitrogen) baculovirus expression system and over-expressed in Sf9 cells as described previously (*1*). Sf9 cells were infected for ~60 hours at 27 ˚C and harvested by centrifugation. Cell pellets were resuspended in Lysis Buffer (50 mM NaH_2PO_4, pH 8.0, 0.3 M NaCl, and 0.5 mM Tris(2-carboxyethyl) phosphine hydrochloride [TCEP]) and lysed in a single pass through an M-110P lab homogenizer (Microfluidics, Westwood, MA). Cellular debris was removed from the soluble lysate via centrifugation and Ago2 was purified from the supernatant solution by incubating with His Select agarose resin (Sigma-Aldrich) for 1.5 hr at 4°C. Contaminating proteins were removed by washing His Select resin with thirty column volumes Wash Buffer (50 mM Tris, pH 8.0, 0.3 M NaCl, 7.5 mM imidazole, and 0.5 mM TCEP). Protein was eluted from the His Select resin in two column volumes of Elution Buffer (50 mM Tris, pH 8.0, 0.3 M NaCl, 0.3 M Imidazole, and 0.5 mM TCEP). Ago2 was visualized on a Commassie stained SDS polyacrylamide gel along side known amounts of BSA, which allowed estimation of the molar concentration of Ago2 in the His Select elution. The synthetic guide RNA (single stranded, 21-nucleotides in length, with a 5'-phosphate) was then added to the nickel purified Ago2 and the resulting mixture was incubated for approximately 15 minutes at 4°C to facilitate guide-loading. The His-tag was removed from Ago2 by the addition of Tobacco Etch Virus (TEV) protease and the resulting Ago2-RNA-TEV mixture was dialyzed overnight at 4°C into HiTrap Buffer (50 mM Tris, pH 8.0, 0.3 M NaCl, 20 mM Imidazole, and 0.5 mM TCEP). Protein contaminants were further removed by passing the dialyzed sample through a 5 ml HiTrap column (GE Healthcare Life Sciences) and collecting the flow-through (unbound) solution. Ago2 molecules loaded with the desired guide RNA were then isolated from those bound to co-purifying cellular small RNAs using the Arpón method, as described previously (*2*). Loaded Ago2 proteins were further purified by size exclusion chromatography using a Superdex 75 10/60 column (GE Healthcare Life Sciences) in SEC Buffer (30 mM CHES, pH 9.0, 1 M NaCl, and 0.5 mM TCEP) to remove contaminating competitor DNA oligonucleotide. The final purified Ago2-guide complex was dialyzed against a solution of 0.1 M NaCl, 0.5 mM TCEP, and 10 mM CHES, pH 9.0, aliquoted, flash frozen in liquid nitrogen, and stored at -80°C. Samples were thawed on ice prior to crystallization and biochemical experiments.

Quantification of Purified Guide-Loaded Ago2

RNA content was determined by quantitative Northern blotting. Guide-loaded Ago2 was boiled in formamide loading buffer (95% formamide, 0.025% (w/v) bromophenol blue, 0.025% (w/v) xylene cyanol FF) and resolved alongside known amounts of free guide RNA by 14% denaturing polyacrylamide gel electrophoresis. RNA was transferred to Hybond-NX membrane (Amersham, GE Healthcare Life Sciences), cross-linked to the membrane with N-(3-Dimethylaminopropyl)-N'-ethylcarbodiimide hydrochloride (*3*) (Sigma) and probed with a complementary ^{32}P-radiolabeled probe in hybridization buffer (0.75 M NaCl, 75 mM Sodium Citrate pH 7.0, 20 mM dibasic sodium phosphate pH 7.2, 7% SDS, 2x Denhardt's Solution, 200 μg salmon sperm DNA (Sigma)). After washing, guide and standard signals were visualized using phosphorimaging and bands quantified using ImageQuant software (GE Healthcare

Life Sciences). Protein concentration of purified Ago2 was determined by Bradford assay (BioRad) using Bovine Gamma Globulin as standard.

The concentration of slicing-competent loaded Ago2 molecules present in purified samples was determined by pre-steady state burst kinetics. 20 nM guide-loaded Ago2 was incubated with 100 nM ^{32}P-radiolabeled target RNA in slicing reaction buffer (20 mM Tris pH 8.0, 0.15 M NaCl, 2 mM $MgCl_2$, 0.5 mM TCEP, 0.01 mg/mL baker's yeast tRNA) at 37°C. For each time point, aliquots were quenched in formamide loading buffer and promptly boiled. All time points were resolved by 14% denaturing polyacrylamide gel electrophoresis. Gels were visualized using phosphorimaging, and uncleaved and product bands quantified using ImageQuant software.

Crystallization and Data Collection

Crystals of guide-loaded Ago2 were grown using hanging drop vapor diffusion at 20 ºC. Drops contained a 1:0.8 ratio of protein (2 mg/mL) to reservoir solution, as described previously (*1*). Ago2-guide-target complexes were formed by the addition of 1.2 molar equivalents of target RNA at room temperature for 10 minutes. Crystals of guide-loaded Ago2 bound to target RNA were grown using hanging drop vapor diffusion at 20 ºC. Drops contained a 1:1 ratio of protein to reservoir solution (16% PEG 3350, 0.1M Tris, pH 8.0, 0.1 M Phenol, 12% Isopropanol, and 10 mM $MgCl_2$) and crystals appeared overnight. Crystals were harvested with nylon loops and flash frozen in liquid N_2. Ago2 mutated to remove sites of phosphorylation from over-expression in Sf9 cells yielded the best diffracting crystals (*1*). Data were collected under cryogenic conditions remotely at beam lines 11-1 and 12-2 at the Stanford Synchrotron Radiation Lightsource (SSRL), and beamline 24-ID-E at the Advanced Photon Source (APS) (*4, 5*). Data were processed using XDS and Scala (*6*-*8*).

Structure Determination

The Ago2-guide-target structure was solved by molecular replacement using individual domains of the guide-only structure (PDB ID 4OLA) as sequential search models with Phaser-MR in the PHENIX graphical user interface (*9*). Models were built using Coot (*10*) and were submitted to XYZ coordinate, TLS, and B-factor refinement using PHENIX. Model building and refinement continued iteratively until all interpretable electron density was modeled. Water molecules were identified automatically in Coot ($2F_{obs}$-F_{calc} map, above 1.8 σ, and greater than 2.4 Å and less than 3.2 Å from hydrogen bond donors or acceptors) and by manual inspection of electron density maps. Magnesium ions were identified manually based on octahedral coordination geometries and difference density peaks greater than 10 σ. Refinement of the guide-only structure used an R_{free} set identical that that used in the original 4OLA refinement. All guide-target structures were refined using a common R_{free} data set. All structure figures were generated with PyMOL (Schrödinger, LLC).

Binding Assays

Guide-loaded Ago2 samples (0–70 nM) were incubated with 0.1 nM ^{32}P-radiolabeled target RNA in binding reaction buffer (30 mM Tris pH 8.0, 0.1 M potassium acetate, 2 mM magnesium acetate, 0.5 mM TCEP, 0.005% (v/v) NP-40, 0.01 mg/mL baker's yeast tRNA (Sigma)), in a reaction volume of 100 µL, for 45 minutes at room

temperature. Using a dot-blot apparatus (GE Healthcare Life Sciences), protein-RNA complexes were captured on Protran nitrocellulose membrane (0.45 μm pore size, Whatman, GE Healthcare Life Sciences) and unbound RNA on Hybond Nylon membrane (Amersham, GE Healthcare Life Sciences). Samples were applied with vacuum and then washed using 100μL of ice-cold wash buffer (30 mM Tris pH 8.0, 0.1 M potassium acetate, 2 mM magnesium acetate, 0.5 mM TCEP). Membranes were air-dried and signals visualized by phosphorimaging. Quantification was performed using ImageQuant software (GE Healthcare Life Sciences), and dissociation constants calculated using Prism version 5.0e (GraphPad Software, Inc.).

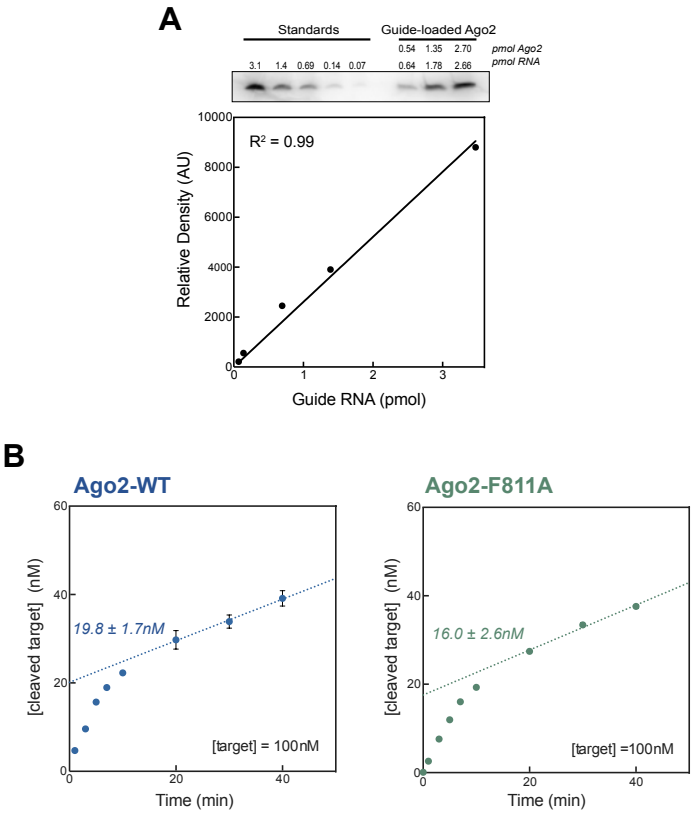

C

Guide	Ago2	Protein concentration by Bradford (mg/mL)	RNA:Protein ratio (Quantitative Northern)	Percent active Ago2 by burst kinetics
Sod1	WT	2.7 ± 0.1	1.2 ± 0.2	99 ± 8.6%
	F811A	5.6 ± 0.1	1.5 ± 0.3	80 ± 13%
miR-122	WT	7.3 ± 0.6	1.2 ± 0.1	-
	F811A	13 ± 2	1.0 ± 0.1	-

Fig. S1

Quantification of guide-selected Ago2. (**A**) RNA content was determined by quantitative northern blotting. Various volumes of guide-selected Ago2 were blotted alongside guide RNA standards (top). Bands were quantified to yield the standard curve (bottom) for determining RNA content in Ago2 samples. RNA:protein were ratios calculated after measuring protein concentration by Bradford assay. (**B**) The amount of catalytically active guide-selected Ago2 molecules present each sample was determined by pre-steady state burst kinetics. Mean values across triplicates are shown inset within graphs ± standard deviation. (**C**) Concentrations, RNA:protein ratios, and percent active molecules of guide-selected Ago2 across preparations with different guides, loaded into wild type or mutant (F881A) Ago2.

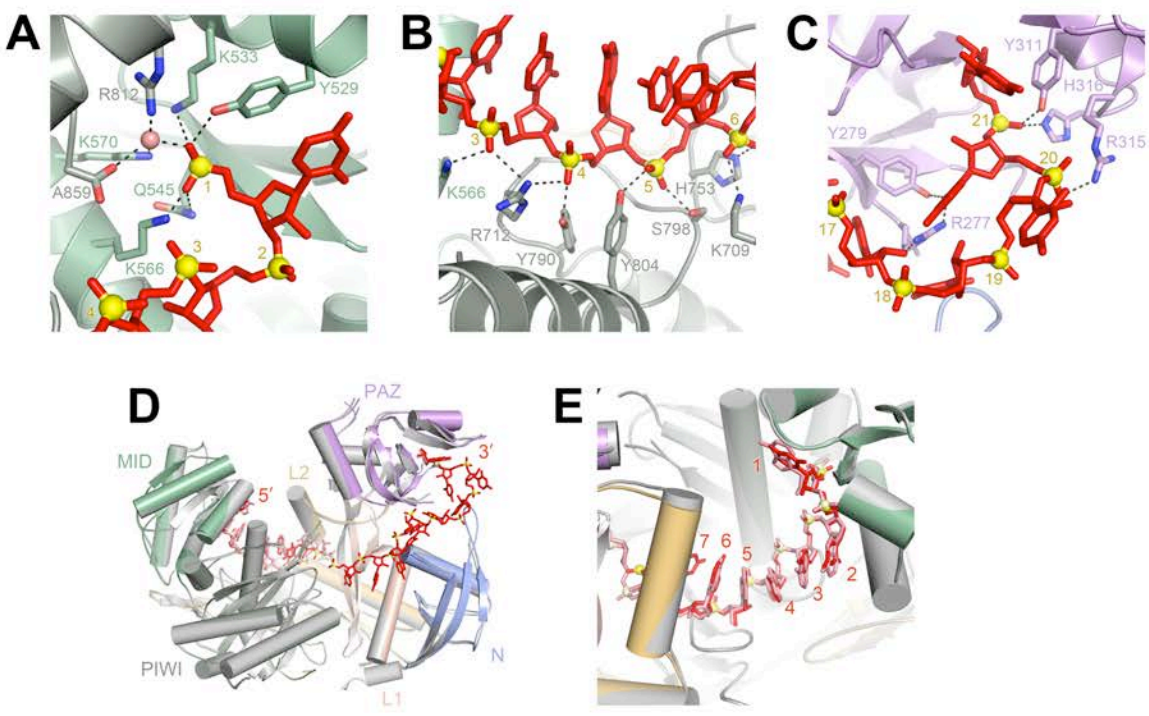

Fig. S2

Details of Ago2-guide interactions. (**A**) Residues Y529, K533, Q545, K566, and K570 of the MID domain, R812 of the PIWI domain, and the carboxy-terminus of the protein make direct contacts to the guide 5'-phosphate. (**B**) Residues K566 of the MID domain and K709, R712, H753, Y790, S798, and Y804 of the PIWI domain make direct contacts to the phosphodiester backbone of nucleotides g3-g6. (**C**) Residues R277, R279, Y311, R315 and H316 of the PAZ domain make direct contacts to the 3' end of the guide RNA. (**D**) Ago2 (colored) bound to a defined guide RNA (red) aligned to Ago2 bound to a mixture of cellular RNAs (grey protein, pink RNA; PDB ID: 4OLA). Except for the appearance of guide nucleotides g12–20 and changes in a few loop residues, the structures are nearly identical (RMSD of 0.415 Å for all equivalent Ca atoms). (**E**) Close up view of overlaid Ago2-guide structures in seed region, colored as in (D).

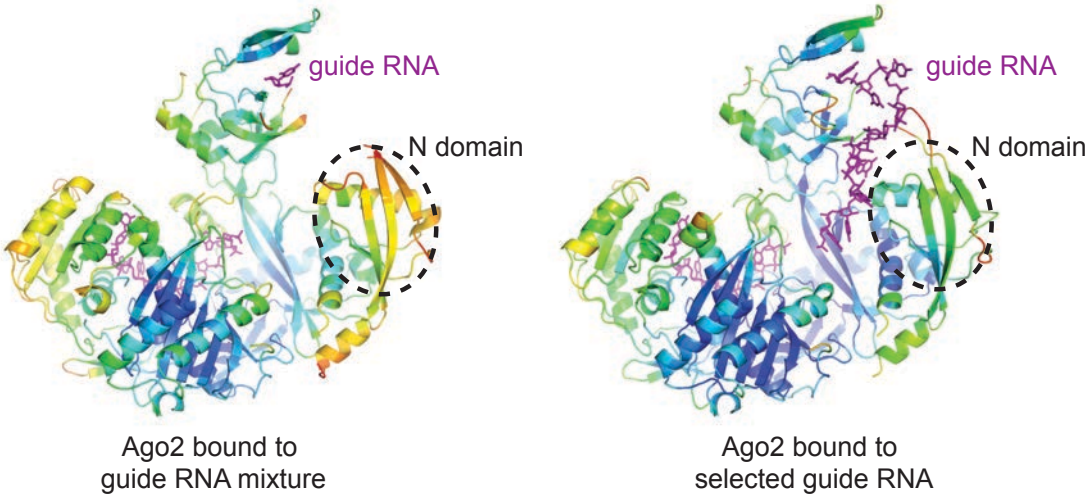

Fig. S3

Ordered guide in guide-selected crystals. Side-by-side comparison of crystal structures of Ago2 bound to a heterogeneous mixture of cellular guide RNAs (left) and Ago2 bound to a homogenous, biochemically-selected guide RNA (right). Proteins colored by relative temperature factors. Guide RNA colored purple.

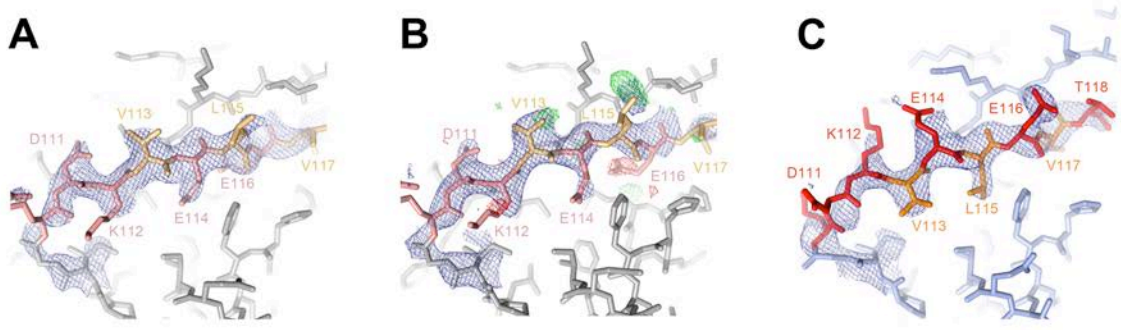

Fig. S4

Correction of mistraced residues 110–118. (**A**) $2F_o$-F_c map (blue mesh) calculated from our original Ago2 data set and refined structure (PDB ID 4EI1) contoured at 1.1σ (prior to corrections). Ago2 is colored in grey with residues 110-117 highlighted with pink hydrophilic side chains and yellow hydrophobic side chains. (**B**) $2F_o$-F_c map (blue mesh) and F_o-F_c map (green and red mesh, contoured at 2.8 and -2.8 σ, respectively) calculated from the original structure and the new, guide-selected data set. Different density indicated that the chain around residues 110-118 had been mistraced in the original structure. (**C**) Shifting 110–118 by one residue satisfied the difference density and reoriented hydrophilic residues (red) towards the bulk solvent and hydrophobic residues (orange) towards the protein interior. The final $2F_o$-F_c map contoured at 1.1σ is shown (blue mesh). Corrected structures have been deposited in the Protein Data Bank (PDB IDs 4EI1 and 4EI3 superseded by 4OLA and 4OLB, respectively).

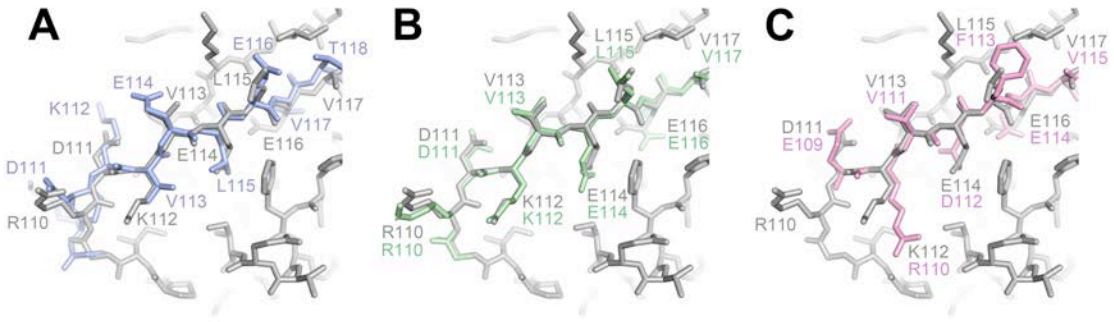

Fig. S5

Propagation of 110–118 errors to subsequent Argonaute structures (**A**) Overlay of the original Ago2 structure (gray) with residues 110–118 from the corrected, guide-selected structure (blue). (**B**) Overlay of the original Ago2 structure (gray) with residues 110–118 from the structure of Ago2 bound to miR-20a (green) (PDB ID 4F3T) reveals the identical error. (**C**) Overlay with the equivalent residues from human Ago1 bound to let-7 (pink) (PDB ID 4KRE) reveals a similar, unlikely placement of hydrophobic and hydrophilic residues, indicating that the original error propagated to this structure as well. In contrast, the human Ago1 structure from Nakanishi and co-workers (PDB ID 4KXT) appears to be traced correctly (not shown).

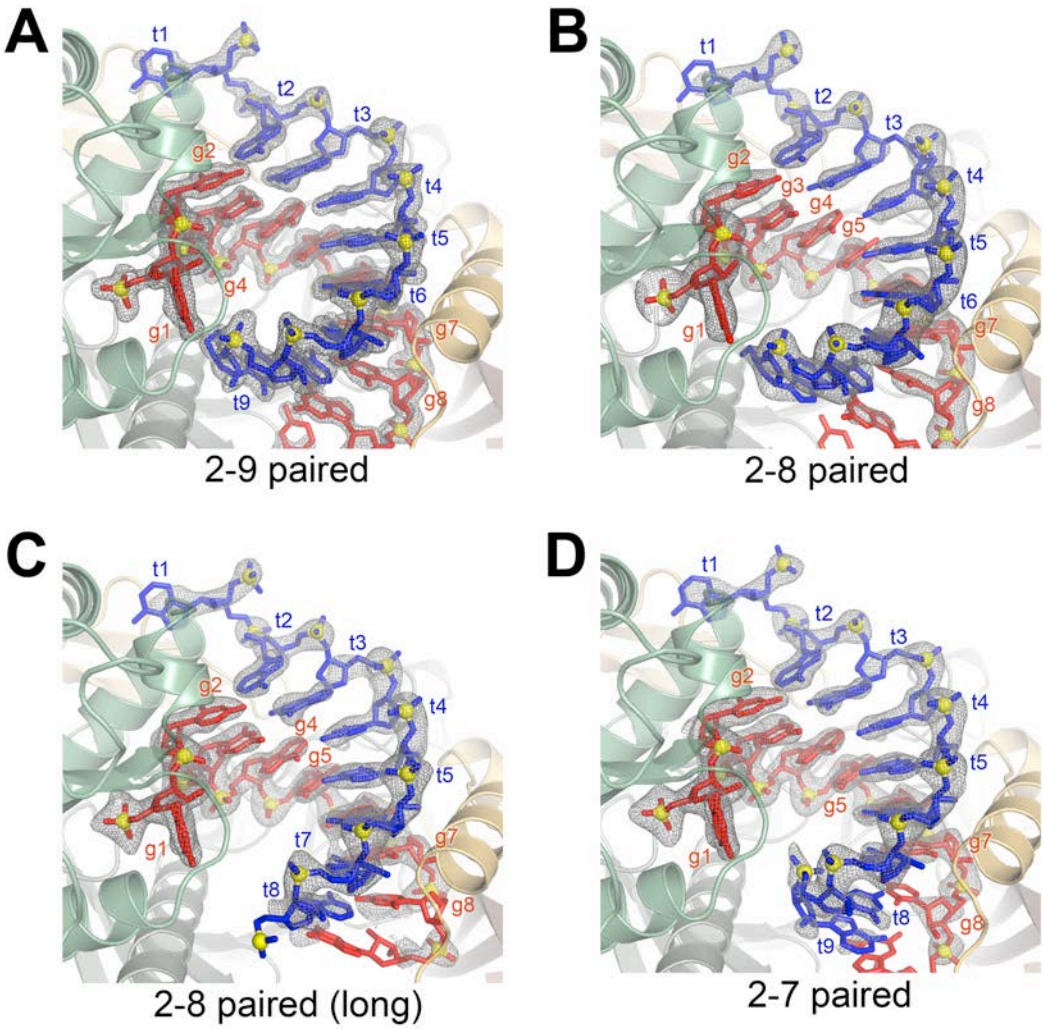

Fig. S6

Omit maps (contoured at 2.5σ) were calculated after refining the final g2-g9 (**A**), g2-g8 (**B**), g2-g8 long (**C**), and g2-g7 (**D**) paired models with all RNA atoms omitted. Electron density for the RNA tended to be strongest in the seed region and weaker, though still interpretable at lower σ values, after position 8.

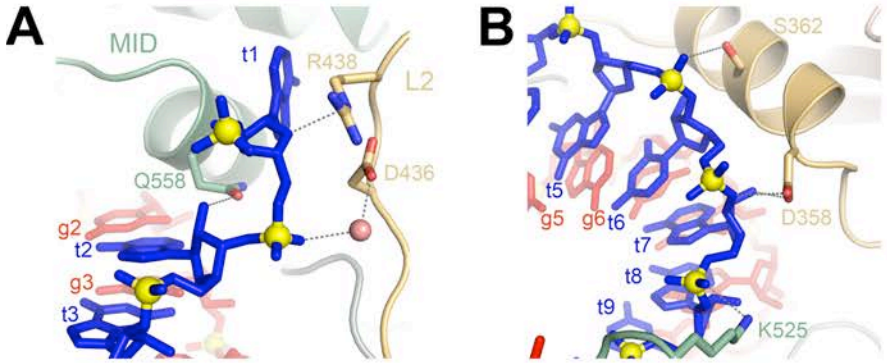

Fig. S7

The L2 linker and MID domains make direct salt linkages to the seed-matched target RNA. (**A**) D436 and R438 contact the t1 sugar and phosphate. Q558 contacts the 2'OH of t2. (**B**) D358, S362, and K525 form hydrogen bonds with the target phosphodiester backbone.

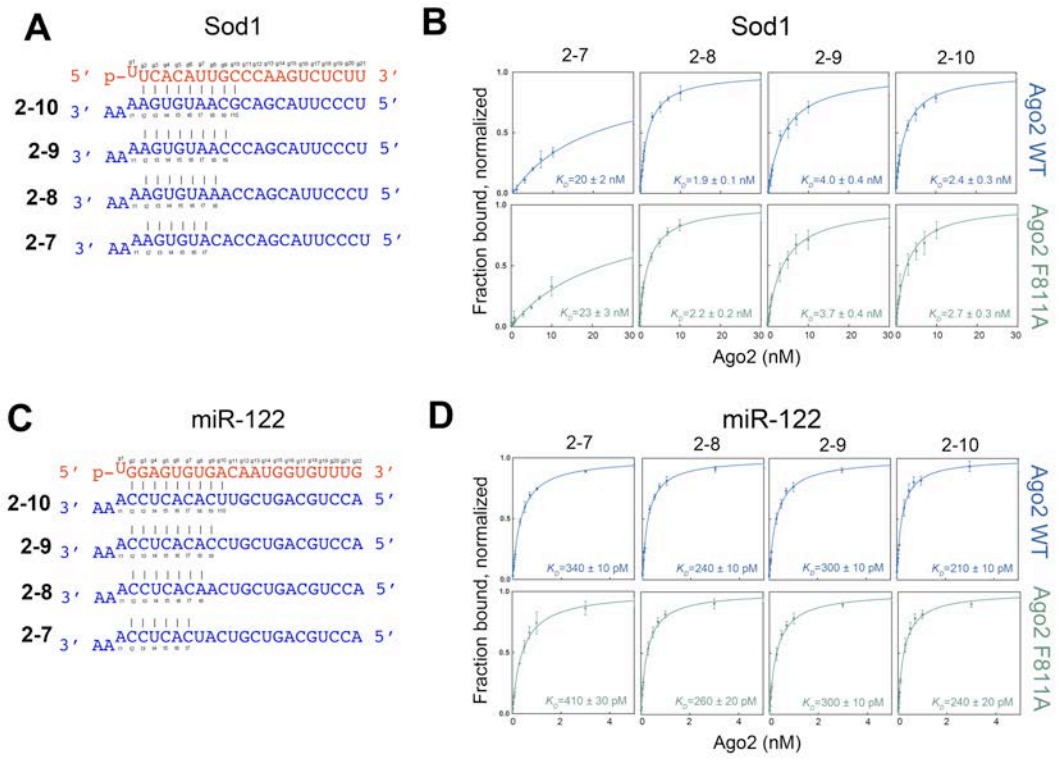

Fig. S8

Target binding data. (**A**) Guide (red) and target (blue) RNA sequences used for binding study 1 (Sod1 guide). (**B**) Equilibrium binding curves for Sod1-selected Ago2, shown for both WT (blue) and F811A mutant (green). Dissociation constants calculated from ≥ three independent replicates, reported ± standard error. (**C**) Guide (red) and target (blue) RNA sequences used for binding study 1 (miR-122 guide). (**D**) Equilibrium binding curves for miR-122-selected Ago2, shown for both WT (blue) and F811A mutant (green). Dissociation constants calculated from ≥ three independent replicates, reported ± standard error.

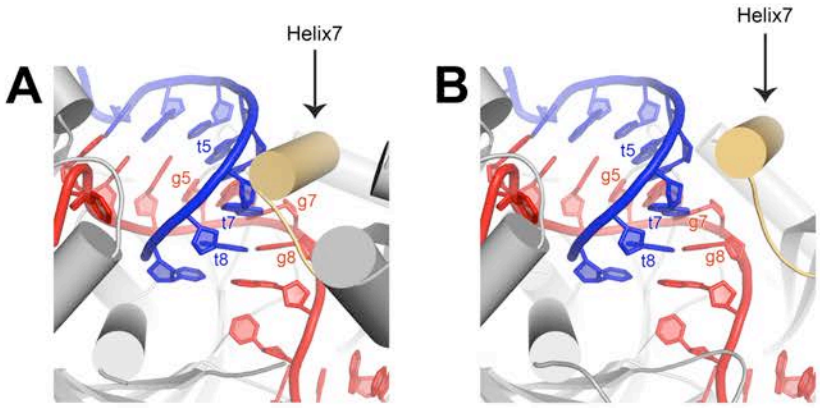

Fig. S9

Helix-7 shifts to accommodate target pairing past g5. (**A**) Helix-7 clashes with target RNA nucleotides t6 and t7 in the Ago2-guide complex conformation. The guide-target duplex (guide, red; target, blue) shown docked into the Ago2-guide structure. Helix-7 is highlighted in yellow. (**B**) Ago2-guide-target crystal structure with helix-7 highlighted, for comparison with panel (A).

Supplemental Discussion:

Comparison of human Ago2 and *T. thermophiles* Ago crystal structures (figs. S10–S12). Comparing structures of human Ago2 to *T. thermophiles* Ago (TtAgo) reveals conserved features and functional differences between these two members of distant branches on the Argonaute protein family tree. These include mechanisms for controlling slicing (fig. S10), conformations of guide RNAs displayed for targeting (fig. S11), conformational changes upon target binding (fig. S12), and interactions with the guide-target duplex (fig. S13).

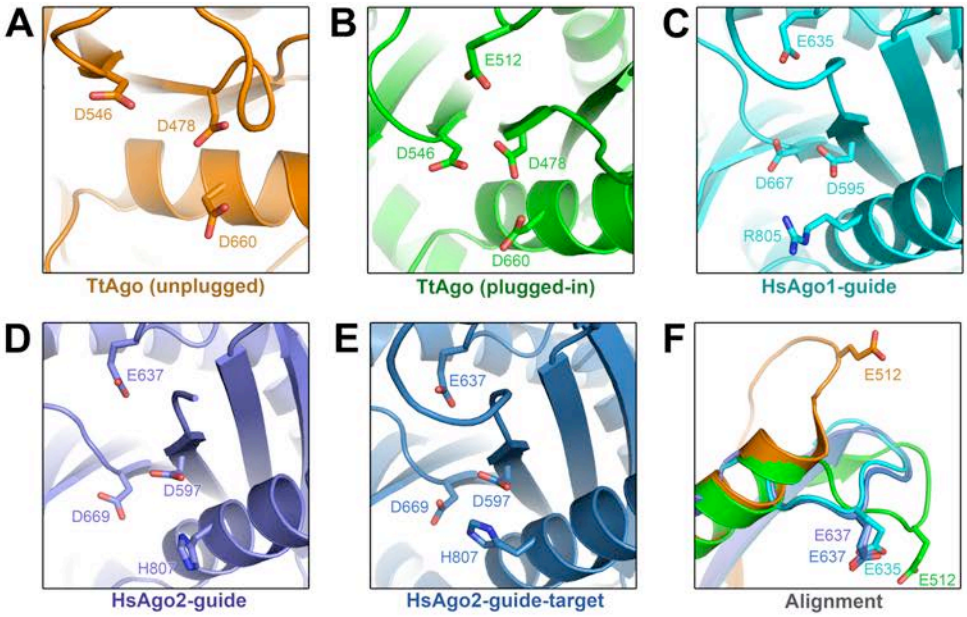

Fig. S10

Active site conformations in bacterial and human Argonauts. (**A**) TtAgo adopts an inactive or "unplugged" conformation (PDB ID 3DLH), with catalytic residue E512 positioned outside of the active site, in the absence of extensive guide-target pairing (*11-13*). (**B**) "Plugged-in" conformation of TtAgo (PDB ID 3HVR), bound to a 19 nt. complementary target (*14*). (**C**) Human Ago1 adopts a plugged-in-like conformation (PDB ID 4KXT), with E635 inserted into the active site, in the absence of target RNA (*11, 15*). (**D** and **E**) Human Ago2 appears in the plugged-in conformation in the absence of target RNA (D), and when bound to seed-paired targets (E). (**F**) Alignment of structures from panels (A–E) in the region surrounding the mobile aspartate residue reveals conformational homogeneity among the human Ago structures, indicating this residue may not plug in and out as shown in TtAgo.

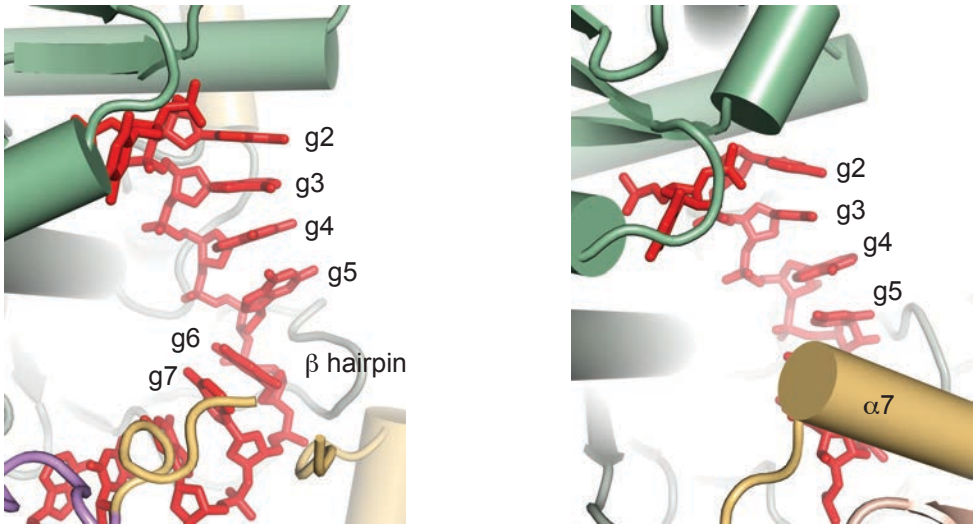

Fig. S11

TtAgo and human Ago2 display guide nt 2–5 for target pairing. Inspection of the TtAgo guide-only structure (*13*) (PDB ID 3DLH) reveals that, like Ago2, TtAgo primarily displays guide nt 2–5 for target pairing. Close examination further reveals that the TtAgo guide contains a distinct kink between nt 4 and 5. The kink appears to be stabilized by an extended beta hairpin composed of residues 605–617. Thus, like eukaryotic Argonautes, the bacterial protein also kinks its guide in the seed region in the absence of target pairing. Furthermore, although TtAgo lacks a structure analogous to helix-7 in Ago2, TtAgo also sterically occludes pairing beyond g5 in the guide-only structure. These observations suggest that, like human Ago2, TtAgo may primarily use guide nt 2–5 for the initial identification of complementary targets. Considering the vast evolutionary distance between these two proteins, we suggest that this is a conserved targeting strategy used by most, if not all, Argonaute proteins.

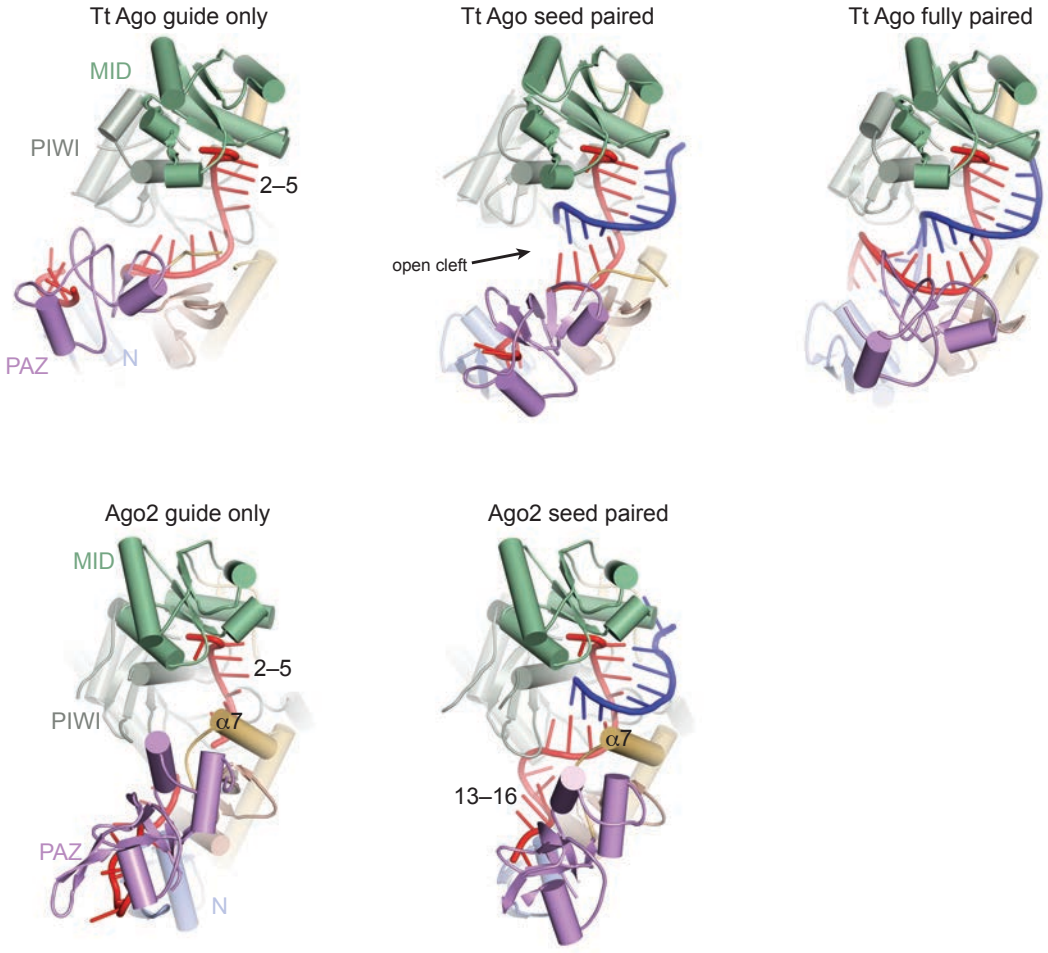

Fig. S12

Conformational changes in TtAgo and human Ago2. The "seed-paired" TtAgo structure (PDB ID 3F73), with target pairing spanning g2–g9, has a significantly widened central cleft compared to the TtAgo guide-only structure (*16*). Seed pairing opens the cleft sufficiently wide to allow extended association of guide and target. Indeed, the conformation of the "fully paired" TtAgo protein (PDB ID 3HK2), with target pairing spanning g2–g16, closely resembles the seed-paired conformation (*14*). In contrast, pairing to the seed region in Ago2 appears to be insufficient to open the central cleft beyond g8. Therefore, a major functional difference between TtAgo and Ago2 appears to be the base pairing requirements for establishing a stably opened central cleft. It is possible that guide-pairing requirements for establishing a stably opened central cleft may differ significantly among other Argonaute proteins as well, which could potentially explain why fly Ago2 and mouse Ago2 behave so differently with regard to extensive complementarity beyond seed paring (*17*).

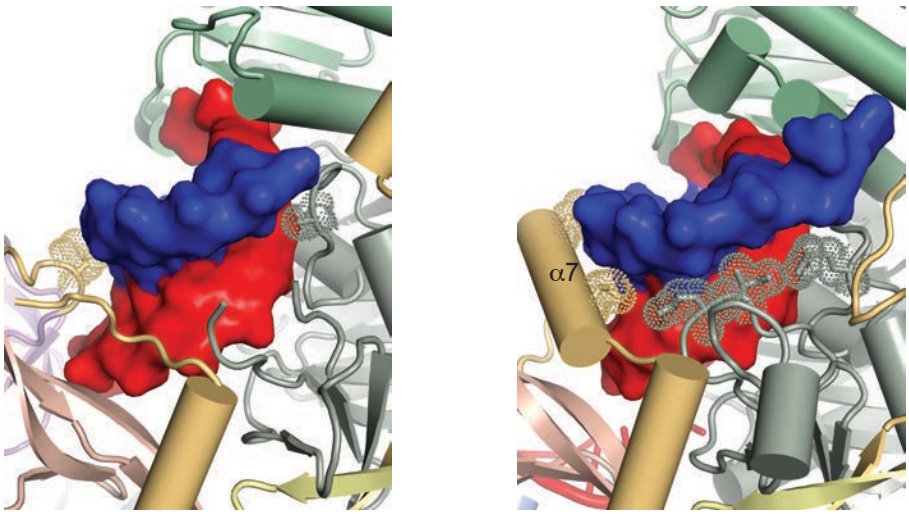

Fig. S13

TtAgo makes fewer minor groove contacts than Ago2. Inspection of the seed paired structure of TtAgo (PDB ID 3F73) reveals that, unlike human Ago2, the bacterial protein does not make extensive contacts to the guide-target minor groove in the seed region. TtAgo lacks a structure analogous to helix-7 in Ago2, and the beta hairpin structure that kinks the TtAgo guide in the guide-only structure (see fig. S11) is disordered in the seed paired structure. Additionally, closer inspection reveals that the guide-target minor groove is wider and deeper in the TtAgo structure than in human Ago2. These differences may reflect functional differences between the two proteins—human Ago2 uses a guide RNA and TtAgo functions with a guide DNA. Moreover, although TtAgo can act on RNA substrates in vitro, the preferred substrate appears to be DNA targets (*14, 18*).

Table S1.
Crystallographic statistics.

Guide: miR-122	K_D **(nM)**	
Positions of guide-target complementarity	*Ago2 WT*	*Ago2 F811A*
2-7	0.34 ± 1	0.41 ± 3
2-8	0.24 ± 1	0.26 ± 2
2-9	0.30 ± 1	0.30 ± 1
2-10	0.21 ± 1	0.24 ± 2
Guide: Sod1	K_D **(nM)**	
Positions of guide-target complementarity	*Ago2 WT*	*Ago2 F811A*
2-7	20 ± 2	23 ± 3
2-8	1.9 ± 0.1	2.2 ± 0.2
2-9	4.0 ± 0.4	3.7 ± 0.4
2-10	2.4 ± 0.3	2.7 ± 0.3
Guide: Sod1	K_D **(nM)**	
t1 nucleotide	*Ago2 WT*	-
A	1.9 ± 0.2	-
G	5.2 ± 1	-
U	5.6 ± 0.9	-
C	5.9 ± 0.4	-

Table S2.
Dissociation constants from target binding experiments.

Movie S1

The PAZ domain and helix7 move as a rigid unit upon target recognition. The Ago2 protein is shown as an interpolation from the guide-only conformation to the guide-target conformation. Nucleic acids removed for clarity.

Movie S2

The animation of the stepwise mechanism for microRNA targeting. Ago2 uses guide nucleotides 2-5 (red) to scan for microRNA targets. A conformational change is induced upon recognition of a target RNA allowing pairing of the guide and target RNAs past guide nucleotide 5. This conformational change results in a widening of the N-PAZ channel, which frees constraints on guide nucleotides 13-16. Guide nucleotides 13-16 shift into the central cleft and adopt an A-form helical conformation with Watson-crick base edges solvent exposed for further pairing to target RNAs.

Supplemental References

1. N. T. Schirle, I. J. MacRae, The crystal structure of human Argonaute2. *Science* **336**, 1037-1040 (2012)..
2. C. F. Flores-Jasso, W. E. Salomon, P. D. Zamore, Rapid and specific purification of Argonaute-small RNA complexes from crude cell lysates. *RNA* **19**, 271-279 (2013).
3. G. S. Pall, C. Codony-Servat, J. Byrne, L. Ritchie, A. Hamilton, Carbodiimide-mediated cross-linking of RNA to nylon membranes improves the detection of siRNA, miRNA and piRNA by northern blot. *Nucleic Acids Res* **35**, e60 (2007)10.1093/nar/gkm112).
4. T. M. McPhillips, S. E. McPhillips, H. J. Chiu, A. E. Cohen, A. M. Deacon, P. J. Ellis, E. Garman, A. Gonzalez, N. K. Sauter, R. P. Phizackerley, S. M. Soltis, P. Kuhn, Blu-Ice and the Distributed Control System: software for data acquisition and instrument control at macromolecular crystallography beamlines. *Journal of synchrotron radiation* **9**, 401-406 (2002).
5. S. M. Soltis, A. E. Cohen, A. Deacon, T. Eriksson, A. Gonzalez, S. McPhillips, H. Chui, P. Dunten, M. Hollenbeck, I. Mathews, M. Miller, P. Moorhead, R. P. Phizackerley, C. Smith, J. Song, H. van dem Bedem, P. Ellis, P. Kuhn, T. McPhillips, N. Sauter, K. Sharp, I. Tsyba, G. Wolf, New paradigm for macromolecular crystallography experiments at SSRL: automated crystal screening and remote data collection. *Acta crystallographica. Section D, Biological crystallography* **64**, 1210-1221 (2008).
6. A. a. T. Gonzalez, Y., in http://smb.slac.stanford.edu/facilities/software/xds/ -autoxds_script. (2010).
7. W. Kabsch, Xds. *Acta crystallographica. Section D, Biological crystallography* **66**, 125-132 (2010).
8. M. D. Winn, C. C. Ballard, K. D. Cowtan, E. J. Dodson, P. Emsley, P. R. Evans, R. M. Keegan, E. B. Krissinel, A. G. Leslie, A. McCoy, S. J. McNicholas, G. N. Murshudov, N. S. Pannu, E. A. Potterton, H. R. Powell, R. J. Read, A. Vagin, K.

S. Wilson, Overview of the CCP4 suite and current developments. *Acta crystallographica. Section D, Biological crystallography* **67**, 235-242 (2011).
9. P. D. Adams, P. V. Afonine, G. Bunkoczi, V. B. Chen, I. W. Davis, N. Echols, J. J. Headd, L. W. Hung, G. J. Kapral, R. W. Grosse-Kunstleve, A. J. McCoy, N. W. Moriarty, R. Oeffner, R. J. Read, D. C. Richardson, J. S. Richardson, T. C. Terwilliger, P. H. Zwart, PHENIX: a comprehensive Python-based system for macromolecular structure solution. *Acta crystallographica. Section D, Biological crystallography* **66**, 213-221 (2010).
10. P. Emsley, B. Lohkamp, W. G. Scott, K. Cowtan, Features and development of Coot. *Acta crystallographica. Section D, Biological crystallography* **66**, 486-501 (2010).
11. K. Nakanishi, M. Ascano, T. Gogakos, S. Ishibe-Murakami, A. A. Serganov, D. Briskin, P. Morozov, T. Tuschl, D. J. Patel, Eukaryote-specific insertion elements control human ARGONAUTE slicer activity. *Cell Rep* **3**, 1893-1900 (2013).
12. G. Sheng, H. Zhao, J. Wang, Y. Rao, W. Tian, D. C. Swarts, J. van der Oost, D. J. Patel, Y. Wang, Structure-based cleavage mechanism of Thermus thermophilus Argonaute DNA guide strand-mediated DNA target cleavage. *Proceedings of the National Academy of Sciences of the United States of America* **111**, 652-657 (2014).
13. Y. Wang, G. Sheng, S. Juranek, T. Tuschl, D. J. Patel, Structure of the guide-strand-containing argonaute silencing complex. *Nature* **456**, 209-213 (2008).
14. Y. Wang, S. Juranek, H. Li, G. Sheng, G. S. Wardle, T. Tuschl, D. J. Patel, Nucleation, propagation and cleavage of target RNAs in Ago silencing complexes. *Nature* **461**, 754-761 (2009).
15. C. R. Faehnle, E. Elkayam, A. D. Haase, G. J. Hannon, L. Joshua-Tor, The making of a slicer: activation of human Argonaute-1. *Cell Rep* **3**, 1901-1909 (2013).
16. Y. Wang, S. Juranek, H. Li, G. Sheng, T. Tuschl, D. J. Patel, Structure of an argonaute silencing complex with a seed-containing guide DNA and target RNA duplex. *Nature* **456**, 921-926 (2008).
17. L. M. Wee, C. F. Flores-Jasso, W. E. Salomon, P. D. Zamore, Argonaute divides its RNA guide into domains with distinct functions and RNA-binding properties. *Cell* **151**, 1055-1067 (2012).
18. D. C. Swarts, M. M. Jore, E. R. Westra, Y. Zhu, J. H. Janssen, A. P. Snijders, Y. Wang, D. J. Patel, J. Berenguer, S. J. Brouns, J. van der Oost, DNA-guided DNA interference by a prokaryotic Argonaute. *Nature* **507**, 258-261 (2014).